Instantaneous Normal Mode Analysis of the Levitation Effect in Zeolites

Sudeshna Kar and Charusita Chakravarty*

Department of Chemistry, Indian Institute of Technology-Delhi, Hauz Khas, New Delhi 110016, India

Received: September 3, 1999; In Final Form: October 25, 1999

An instantaneous normal mode (INM) analysis of the levitation effect in zeolites is presented in this paper. Lennard-Jones sorbates of variable size and polarizability diffusing in Na−Y zeolite are studied using microcanonical molecular dynamics (MD) simulations. A comparison of the dynamical information from the MD simulations with predictions based on INM analysis shows that the INM spectrum carries several striking signatures of the levitation effect. The fraction of imaginary modes mirrors the trend in the diffusion coefficient as a function of sorbate size and shows an anomalous levitation peak. The Einstein frequency, as a function of sorbate size, shows a minimum at the position of the anomalous peak. The qualitative shape of the INM spectrum changes in the anomalous regime, reflecting the availability of 12-ring window sites for adsorption, in addition to the α-cage sites. The velocity autocorrelation functions of the sorbate are well-reproduced from INM data for short time scales of one picosecond, particularly in the anomalous regime. The time of crossover from ballistic to diffusional motion can be approximately predicted from INM spectra since it is found to be similar to the time at which the velocity autocorrelation function first turns negative. These results lead one to expect that the INM spectrum, though an equilibrium static property of the system, can be used very effectively as an indicator of qualitative changes in diffusional dynamics of sorbates in porous media.

1. Introduction

Transport properties of fluids confined in microporous solids is a subject of considerable experimental and theoretical interest.[1−5] The practical importance stems from the widespread use of microporous materials as molecular sieves and shape selective catalysts. Theoretically, the relationship between dynamical properties of a confined fluid and properties of the confining medium, such as its geometry, composition, and degree of disorder, is still not well-understood. Rare-gas/zeolite systems are among the simplest sorbate/sorbent systems which are both amenable to detailed simulation studies and which display interesting dynamical features due to confinement. Rare gases as sorbates are characterized by two parameters: (i) the size or van der Waals radius which determines its geometric properties in relation to the sorbent and (ii) the polarizability which determines the strength of interaction with the confining medium. Zeolites are convenient sorbents for study because they have well-characterized, ordered structures and display a wide range of pore sizes, channel geometries, and network topologies. Over the past decade, simulation studies of rare-gases in zeolites have uncovered several unexpected dynamical phenomena such as single-file diffusion,[6,7] levitation effect,[8−15] and quantum sieving.[15] In this work, we focus on an analysis of the levitation effect using instantaneous normal mode analysis.[16]

A given zeolite can act as a sieve for sorbates with dimensions smaller than the narrowest portion of the connecting channels or windows. A simple geometric picture of diffusional behavior would also lead one to expect that the self-diffusion coefficient *D* will be maximum for very small sorbates and will decrease with increase in sorbate size. This is in fact observed in most MD simulations of simple sorbates in zeolites. However, under certain circumstances, a nonmonotonic increase in *D* with increasing sorbate size is observed for sizes close to the minimum channel width. This anomalous peak in transport properties has been termed the levitation effect.[8−15] The levitation effect has been demonstrated in MD simulations of Lennard-Jones sorbates in a number of zeolites, such as Na−Y, Na-A, silicalite and VPI.[8−11] Since the effect generally becomes more pronounced as temperature or concentration are decreased, it would appear to be strongly correlated with the potential energy surface imposed on the sorbate by the confining medium. A detailed study of adsorption sites and minimum energy pathways of Lennard-Jones sorbates in Na−Y indicates that the onset of the levitation effect can be correlated with the availability of additional absorption sites in the windows of the sodalite cages.[12]

The possibility of a close connection between the levitation effect and the topography of the potential energy surface (PES) led us to perform an instantaneous normal mode (INM) analysis. The INM spectrum is obtained as the set of normal mode frequencies associated with configurations sampled from some suitable ensemble.[17−19] Therefore, the INM spectrum closely reflects the curvature distribution of the potential energy surface as sampled by the system. Moreover, the INM frequencies are related to the short-time dynamics since for sufficiently small displacements and therefore for sufficiently small times, a quadratic expansion of the potential about any reference configuration will be adequate. This has been borne out by simulations on a wide range of systems, including atomic clusters, molecular liquids, liquid metals and ionic melts.[20−26] Recent work indicates that INM analysis is a good predictor of short-time dynamical behavior for rare gases confined in zeolites.[27−29] For example, the fraction of imaginary modes was found to be strongly correlated with the self-diffusion coefficient and the short-time behavior of the velocity autocorrelation function was well reproduced by the INM expression, particu-

* Author for correspondence.

10.1021/jp993137o CCC: $19.00
Published on Web 01/07/2000

larly at low temperatures. Therefore it is reasonable to expect that if the levitation effect is strongly determined by the nature of the potential energy surface, it should be associated with signatures in the INM spectrum.

In this work, we consider the levitation effect for Lennard-Jones sorbates of variable size and polarizability diffusing in Na−Y zeolite. Dynamical information from molecular dynamics simulations is compared with predictions based on instantaneous normal mode analysis. The INM spectrum is shown to carry several striking signatures of the levitation effect.

The paper is organized as follows. Aspects of instantaneous normal mode analysis relevant for this study are summarized in section 2. Simulation methods and computational details are given in section 3. Results and discussion are presented in section 4 and Conclusions in section 5.

2. Instantaneous Normal-Mode Analysis

An instantaneous normal mode analysis is performed by expanding the potential energy function to second order in the displacement, $\mathbf{r}(t) - \mathbf{r}(0)$, where $\mathbf{r}(0)$ is the initial configuration of the N-particle system at time $t = 0$ and $\mathbf{r}(t)$ is the configuration after a short interval of time t. The short-time classical Hamiltonian can then be written as

$$H \approx \sum_{i=1}^{3N} \frac{m_i}{2}\left(\frac{\mathrm{d}r_i}{\mathrm{d}t}\right)^2 + \mathbf{V}(\mathbf{r}(0)) - \mathbf{F}'\cdot(\mathbf{r}(t) - \mathbf{r}(0)) + 0.5(\mathbf{r}(t) - \mathbf{r}(0))^{\mathrm{T}}\cdot\mathbf{D}'\cdot(\mathbf{r}(t) - \mathbf{r}(0)) \quad (1)$$

where $\mathbf{F}'$ is the vector representing the forces acting on the system at $t = 0$ and $\mathbf{D}'$ is the second-derivative matrix or Hessian of the potential evaluated at $\mathbf{r}(0)$. Converting to mass-weighted coordinates, $z_i = \sqrt{m_i} r_i$,

$$H \approx \sum_{i=1}^{3N} \frac{1}{2}\left(\frac{\mathrm{d}z_i}{\mathrm{d}t}\right)^2 + V(\mathbf{r}(0)) - \mathbf{F}\cdot(\mathbf{z}(t) - \mathbf{z}(0)) + 0.5(\mathbf{z}(t) - \mathbf{z}(0))^{T}\cdot\mathbf{D}\cdot(\mathbf{z}(t) - \mathbf{z}(0)) \quad (2)$$

where the derivative matrixes $\mathbf{F}$ and $\mathbf{D}$ are constructed with respect to the mass-weighted coordinates. The Hessian matrix can be diagonalized to give the eigenvalues, ω_i^2, $\{i = 1, 3N\}$, and eigenvectors $\mathbf{U}(\mathbf{r}(0))$. The eigenvalues correspond to the squares of the normal mode frequencies and may be positive or negative corresponding to real and imaginary frequencies respectively. Conventionally the imaginary branch is depicted on the negative frequency axis.

The INM spectrum or the normalized INM density of states is obtained by averaging the INM frequencies over a set of configurations sampled from the equilibrium distribution in any ensemble. Mathematically, it may be represented as

$$\rho(\omega) = \langle (1/3N) \sum_{i=1}^{3N} \delta(\omega - \omega_i) \rangle \quad (3)$$

The equilibrium INM spectrum can be defined in any ensemble and for both quantum and classical systems. The fraction of imaginary modes F_{imag} indicates the extent to which the system samples regions of negative curvature, including barrier and shoulder regions of the potential energy surface. The Einstein frequency ω_{E} is defined as: $\omega_{\mathrm{E}}^2 = \int \omega^2 \rho(\omega)\, \mathrm{d}\omega$ where $\rho(\omega)$ is the normalized INM spectrum. Since $\omega_{\mathrm{E}}^2 = \langle V'' \rangle / m(3N - 3)$, where $\langle V'' \rangle$ is the ensemble average of the trace of the Hessian $\mathbf{D}'$, the Einstein frequency is a measure of the average force constant, $\langle V'' \rangle / ((3N - 3)$, of the system. ω_{E} can be decomposed into real ω_{R} and imaginary ω_{I} components such that

$$\omega_{\mathrm{E}}^2 = (1 - F_{\mathrm{imag}})\omega_{\mathrm{R}}^2 + F_{\mathrm{imag}}\omega_{\mathrm{I}}^2 \quad (4)$$

where F_{imag} is the fraction of imaginary frequencies.

For a classical system, it is possible to obtain an approximation to the short-time dynamics in terms of the kinematics of the normal mode coordinates. By using the INM modes, $U(\mathbf{r}(0))$ for some configuration, $\mathbf{r}(0)$, one can rewrite the Hamiltonian as

$$H \approx V(\mathbf{r}(0)) + \sum_{i=1}^{3N}\left(\frac{1}{2}\left(\frac{dq_i}{dt}\right)^2 + \frac{1}{2}\omega_i^2 q_i^2 - f_i q_i\right) \quad (5)$$

where $f_i(\mathbf{r}(0)) = \sum_j U_{ij} F_i$ and $q_i(t,\mathbf{r}(0)) = \sum_j U_{ij}\{z_j(t) - z_j(0)\}$. To remove the term linear in $\{q_i\}$ from the Hamiltonian, one can define shifted normal mode coordinates, $x_i = q_i - (f_i/\omega_i^2)$, such that

$$H \approx V(\mathbf{r}(0)) + \sum_{i=1}^{3N}\left(\frac{1}{2}\left(\frac{dx_i}{dt}\right)^2 + \frac{1}{2}\omega_i^2 x_i^2 - (f_i^2/2\omega_i^2)\right) \quad (6)$$

$|f_i/\omega_i^2|$ can be interpreted as the displacement of the normal mode coordinate from its nearest extremum: minimum in the case of stable modes with $\omega_i^2 > 0$ and maximum in the case of unstable modes with $\omega_i < 0$. The time evolution of the shifted normal modes and the corresponding velocities are given by

$$x_i(t) = x_i(0)\cos(\omega_i t) - (v_i(0)/\omega_i)\sin(\omega_i t)$$

$$v_i(t) = v_i(0)\cos(\omega_i t) - \omega_i x_i(0)\sin(\omega_i t)$$

Using these relations for the time evolution and assuming a Maxwell−Boltzmann distribution of velocities at $t = 0$, Stratt et al. have shown that the velocity autocorrelation function is given by

$$C_{vv}(t) = \int \rho(\omega)\cos(\omega t)\mathrm{d}\omega = 1 - \frac{\langle\omega^2\rangle}{2!}t^2 + \frac{\langle\omega^4\rangle}{4!}t^4 + \ldots \quad (7)$$

where $\langle\omega^n\rangle = \int \omega^{\mathrm{n}}\rho(\omega)\mathrm{d}\omega$. For simple liquids and for rare gases in zeolites, the short time behavior of the translational autocorrelation function is well reproduced by the above formula provided only stable modes are used for evaluating the integral.

3. Computational Details

3.1. Potential Energy Surfaces. The potential energy function for Lennard-Jones sorbates in Na−Y is identical to that used in previous studies of the levitation effect.[10,12] The total potential energy of the system is subdivided into a guest−host term, U_{gh}, which represents the interaction between the sorbate or guest atom with the host lattice and a guest−guest term, U_{gg}, which is a pairwise Lennard-Jones interaction between the sorbate atoms. As in previous studies, the induction term due to interaction between the polarizable sorbate and framework charges is neglected and only the dispersion interaction is retained. The functional form of the potential is based on the

TABLE 1: Self-Interaction Lennard-Jones Potential Parameters Used in Constructing the Kiselev Potential Energy Function

type	σ (Å)	ϵ (K)	ϵ (kJ mol^{-1})
Xe−Xe	4.1	221	1.8378
O−O	2.5447	155.02	1.2891
Na−Na	3.369378	4.714	0.0392

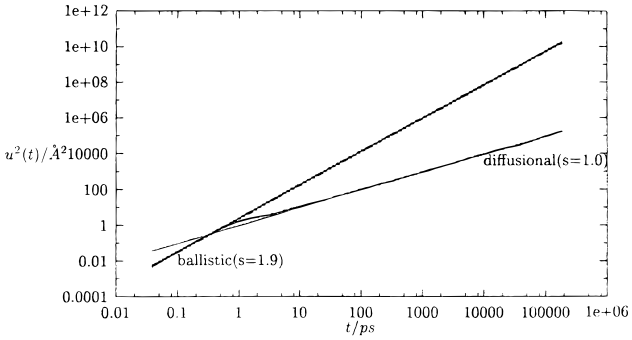

Figure 1. Cross over from ballistic to diffusional motion as seen in the ln−ln plot of $u^2(t)$ (in Å^2) versus t (in picoseconds) for $\sigma_{SS} = 4.1$, $\epsilon_{SS} = 221$ K, and $T = 190$ K.

Kiselev model[30−32] and is given by

$$V = \sum_{l}\sum_{j=1}^{n_l} 4\epsilon_{lS}\sum_{j=1}^{N}\left(\frac{\sigma_{lS}^{12}}{r_{ij}^{12}} - \frac{\sigma_{lS}^{6}}{r_{ij}^{6}}\right) \tag{8}$$

where l numbers the types of atoms present other than tetrahedral atoms such as Si or Al, N is the total number of sorbate atoms, n_l is the number of atoms of type l, r_{ij} is the distance between sorbate atom i and lattice atom j, and ϵ_{lS} and σ_{lS} are Lennard-Jones parameters for interaction between lattice atom of type l and the sorbate S. In the case of Na−Y zeolite, given the LJ parameters for the O−O, Na−Na, and S−S interactions (see Table 1), the appropriate values of ϵ_{lS} and σ_{lS} can be computed using the Lorentz−Berthelot combination rules: (i) $\epsilon_{lS} = \sqrt{\epsilon_{ll}\epsilon_{SS}}$ and (ii) $\sigma_{lS} = 0.5(\sigma_{ll} + \sigma_{SS})$.[32] LJ parameters for O−O and Na−Na interactions are kept constant. At a given value of ϵ_{SS}, σ_{SS} is varied between 2.67 and 7.0 Å, and the s_{OS} and σ_{NaS} values are correspondingly altered. Note that ϵ_{SS} and σ_{SS} values for Xenon are 4.1 and 221 K, respectively.[33]

Zeolite NaY belongs to the space group $Fd\bar{3}m$ with lattice parameter 24.85 Å and unit cell composition $Na_{48}Si_{144}Al_{48}O_{384}$.[34] It is a high-porosity zeolite with large α-cages approximately 11.8 Å in diameter, in addition to the smaller β or sodalite cages. Each α-cage is tetrahedrally connected to four other α-cages by windows of approximately 8 Å diameter formed by 12 oxygen atoms.

3.2. Simulation Details. *3.2.1. Molecular Dynamics.* Molecular Dynamics (MD) simulations were carried out in the microcanonical (NVE) ensemble using the velocity Verlet algorithm.[35,36] Initial velocities were sampled from a Maxwell−Boltzmann distribution corresponding to some preset temperature and then temperature scaling was carried out during the equilibration period. In keeping with previous studies,[10] the preset temperature was fixed at 190 K; the mean temperatures in all the runs were within ±5 K of this value. A single unit cell of Na−Y zeolite was taken as the simulation cell. Eight Lennard-Jones sorbate atoms of mass 131 amu were loaded in each simulation cell. Cubic periodic boundary conditions were imposed. A spherical cutoff radius of 12 Å was employed for sorbate−sorbate and sorbate−zeolite interactions. A timestep of 800 au(19.2 fs) was found to conserve energy to better than the third significant figure for a run length of 192 ns and was used for all the simulations. Runlengths ranged from 1.92 to 192 ns. A rigid zeolite framework was assumed in our simulations to ensure consistency with earlier studies of the levitation effect.[11−13] Instantaneous normal modes were calculated at intervals of 100 timesteps. The INM spectra results from MD at the average temperature of the run T_r coincided with canonical MC results at the same temperature within the error bars of the simulation.[28]

3.2.2. Crossover from Ballistic to Diffusional Motion. The mean squared displacement $u^2(t)$ may be defined as

$$u^2(t) = \langle |r_i(t) - r_i(0)|^2 \rangle \tag{9}$$

$$= 1/N\sum_{i=1}^{N}\frac{1}{(t_{max} - t)}\int_0^{t_{max}-t}[\vec{r}_i(t+\tau) - \vec{r}_i(\tau)]^2\, d\tau \tag{10}$$

where t_{max} is the duration of the simulation. A plot of the mean-squared displacement u^2 versus time t can be subdivided into two distinct regimes: (i) the initial ballistic regime for which $u^2 \propto t^2$ and (ii) the diffusional regime with $u^2 \propto t$.[37] Figure 1 shows the log−log plots of $u^2(t)$ versus t for Xenon ($\sigma_{SS} = 4.1$ and $\epsilon_{SS} = 221$ K) in Na−Y. In all the cases studied, the time period till approximately 1 ps can be definitely classed as in the ballistic regime, while beyond 50 ps, the system is definitely in the diffusional regime. It can be seen that there is a short crossover region rather than a unique cross-over time. To obtain a reasonable approximation to the crossover time τ_c, a least-squares-fitting procedure was used to obtain straight line fits in the two regions and the point of intersection of the two lines was taken to be τ_c.

3.2.3. Computation of Diffusion Coefficient. We have used an order-N algorithm[36] to calculate the self-diffusion coefficient D using the Einstein relation:

$$D = (1/3)\int_0^{t_{max}} dt\langle v_i(t)v_i(0)\rangle \tag{11}$$

Convergence of the diffusion coefficient was tested with respect to run lengths by computing D for each sorbate size and polarizability for run lengths of 1.92, 19.2, and 192 ns. Reported values of D correspond to those calculated from the runs of longest length. Error bars on D for these runs are of the order of ±10%.

4. Results and Discussion

4.1. Signatures of the Levitation Peak in the INM Spectra. The levitation peak has been defined as an anomalous peak in the values of various transport coefficients, primarily the self-diffusion constant D as a function of sorbate size. In this section, we consider two significant properties which characterize the INM spectrum: the fraction of imaginary modes, F_{imag} and the Einstein frequency ω_E as a function of sorbate size.

Figure 2a shows the variation of the self-diffusivity D as a function of $1/\sigma_{SS}^2$ for $\epsilon_{SS} = 221$ K and reproduces the earlier results of Yashonath and Santikary.[10] The position of the levitation peak at $\sigma_{SS} = 6$ Å is the same in the two studies. Differences observed in the values of D between their work and ours may be attributed to statistical errors. It may be noted that the earlier study used much shorter run lengths of 2.6 ns.

Figure 2b shows the fraction of imaginary modes F_{imag} as a function of $1/\sigma_{SS}^2$. It is observed that the fraction of imaginary modes essentially mirrors the behavior of the diffusion coefficient as a function of sorbate size. An anomalous peak in F_{imag}

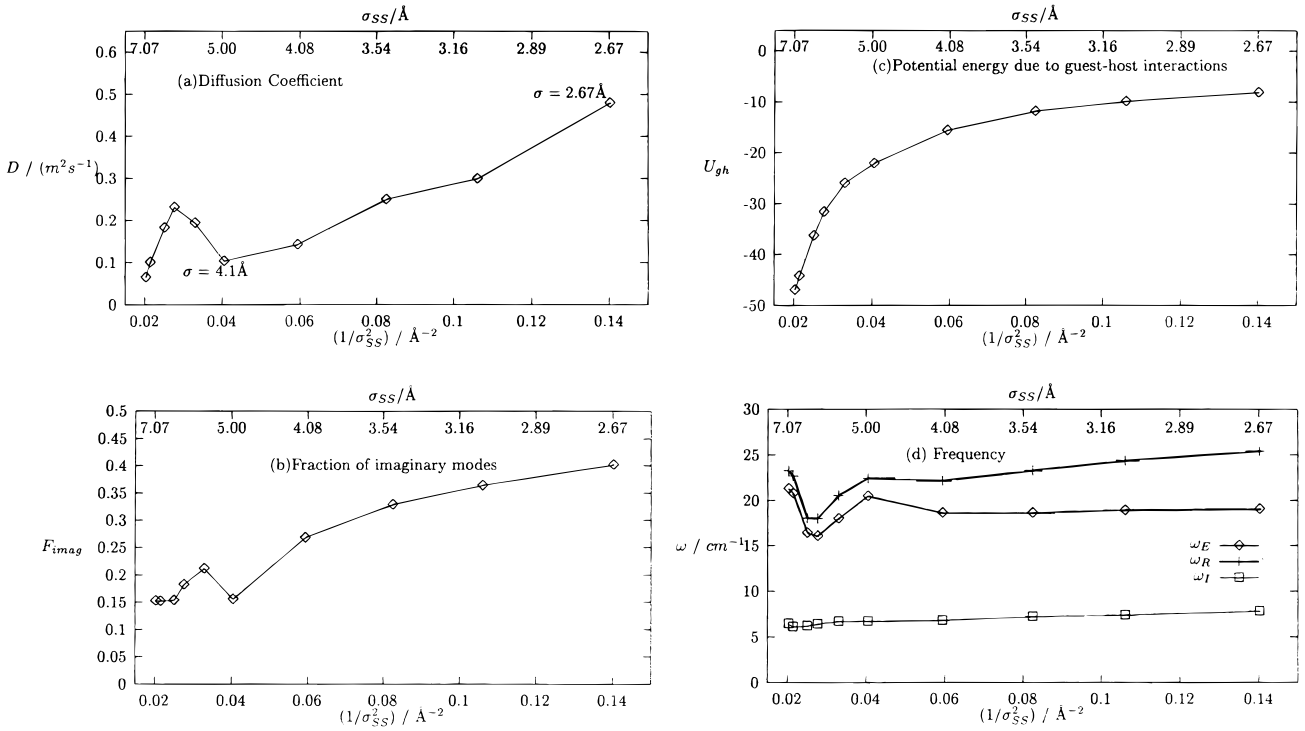

Figure 2. Variation with $1/\sigma_{SS}^2$ of (a) self-diffusivity, D (b) fraction of imaginary modes F_{imag}, (c) guest−host potential energy $\langle U_{gh} \rangle$, (d) the Einstein frequency ω_E, the average real frequency ω_R, and average imaginary frequency ω_I. ϵ_{SS} is fixed at 221 K and temperatures for all the runs are held at 190 ± 5 K.

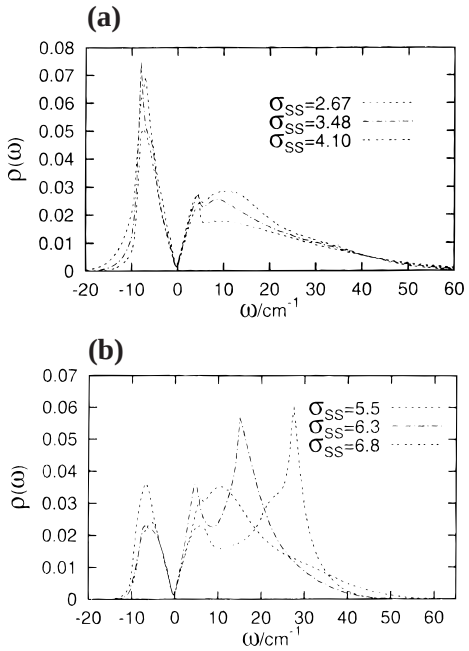

Figure 3. Instantaneous normal mode spectra for different sorbate sizes in the (a) linear regime and (b) anomalous regime. ϵ_{SS} is fixed at 221 K and temperatures for all the runs are held at 190 ± 5 K.

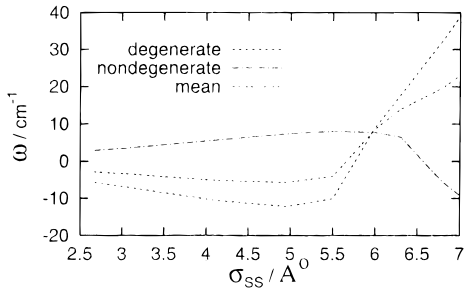

Figure 4. Normal mode frequencies of a single Lennard-Jones sorbate located in the center of a 12-ring window connecting two adjacent α-cages, shown as a function of sorbate size, σ_{SS} for ϵ_{SS} = 221 K. The frequencies of the doubly degenerate in-plane sorbate vibration and the nondegenerate out-of-plane vibration are shown separately. Also shown is the mean of the three sorbate frequencies.

is seen at σ_{SS} = 5.5 Å which may be compared with the peak position at 6 Å in Figure 2a. Thus the INM spectrum contains a very clear signature of the levitation effect and confirms previous observations that the fraction of imaginary modes and the self-diffusivity coefficient are closely correlated. Moreover, the position of the levitation peak is clearly related to the extent of negative curvature of the potential energy surface, rather than to the magnitude of the guest−host binding energy. This may be seen by comparing Figure 2a with Figure 2c, which shows that the average guest−host potential energy U_{gh} decreases smoothly with $1/\sigma_{SS}^2$ and is clearly uncorrelated with the levitation peak.

To support the correlation between the levitation effect and the curvature distribution of the potential energy surface, Figure 2d shows the variation of the Einstein frequency ω_E with sorbate size since ω_E is proportional to the average curvature of the potential energy surface. Also shown are the average frequencies of the real and imaginary branches of the INM spectrum. All three frequencies show a positive correlation with each other. It is notable that all the three frequencies show a trough as a function of $1/\sigma_{SS}^2$ at the position of the anomalous peak in D. The trough is more pronounced for ω_E and ω_R than ω_I. Thus the anomalous peak is associated with a minimum value for the average force constant of the system and a maximum value for the fraction of imaginary modes.

4.2. INM Spectra. In this section, we consider the actual INM spectral distributions rather than properties averaged over the INM distribution, as done in the previous section. Figure 3a shows INM spectra for three values of σ_{SS} which lie in the

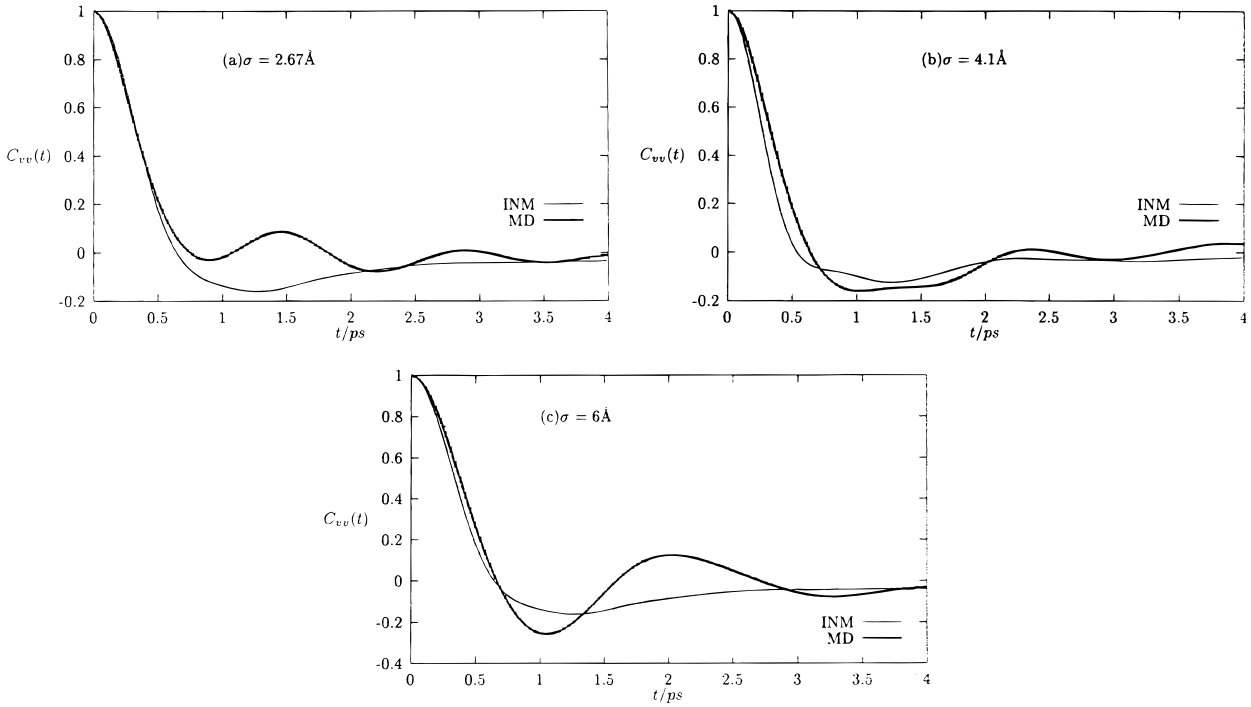

Figure 5. Comparison of velocity autocorrelation functions calculated using MD and INM approaches for σ_{SS} values of (a) 2.67 Å, (b) 4.1 Å, and (c) 6.0 Å. ϵ_{SS} is fixed at 221 K, and temperatures for all the runs are held at 190 ± 5 K.

linear regime. All three INM spectra are qualitatively similar though the imaginary branch intensity decreases with increasing σ_{SS}. As σ_{SS} increases, the peak of the real branch shifts to higher frequencies. Figure 3b shows the INM spectrum for three sorbate sizes in the anomalous regime. The onset of the anomalous rise in D is signaled by the formation of a shoulder in the real branch of the INM spectrum at 5.5 Å. Further increase in sorbate size leads to a broadening of the shoulder and then the formation of a second peak, as seen in the case of $\sigma_{SS} = 6.3$ Å. The position of this second peak moves to higher frequencies as the sorbate size increases.

The formation of the second peak can be explained using the fact that as the system parameters are tuned to move into the anomalous diffusional regime. A second adsorption site opens up at the center of the 12-ring window in addition to sites within the α-cage.[12] Since the sorbate atom can then occupy distinct cage and window sites, the INM spectrum becomes a double-peaked structure. To demonstrate this connection, we have computed the three normal mode frequencies of a Lennard-Jones sorbate located at the center of one of the 12-ring windows. Figure 4 shows the frequencies of the out-of-plane and doubly degenerate in-plane vibrations as a function of sorbate size. It is seen that as we move into the anomalous regime, the degenerate in-plane frequency as well as the mean frequency of vibration of the sorbate atom in the window cage increases sharply indicating stronger localization of the sorbate atoms in the window site. The positions of the second peak in the INM spectrum for $\sigma_{SS} = 6.3$ Å and 6.8 Å coincide with the frequency of the in-plane doubly degenerate vibration, as shown in Figure 4.

4.3. Velocity Autocorrelation Function. The strong signatures of the levitation effect seen in the INM spectrum, indicate that a more detailed investigation of the short-time dynamical information contained in the spectrum is warranted. Previous studies show that the short-time behavior of the velocity autocorrelation function or vacf, $C_{vv}(t)$, is well-reproduced from INM data, particularly at low temperatures.[28] Figure 5a,b,c show

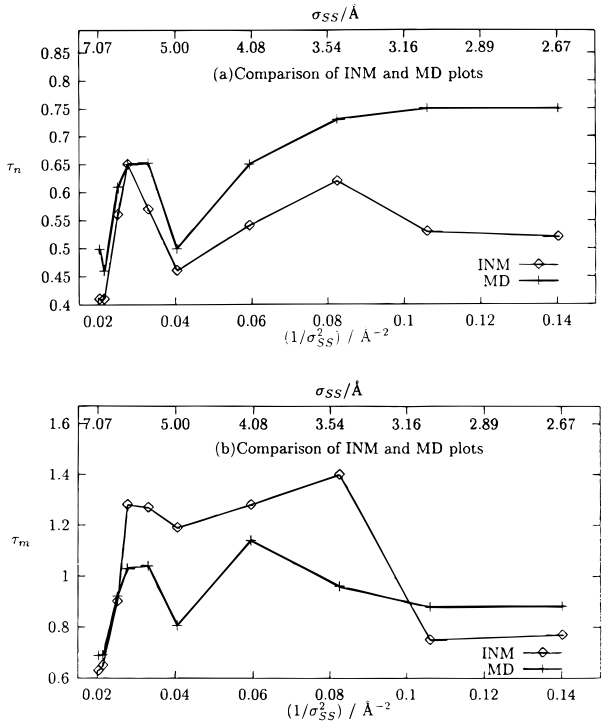

Figure 6. Comparison of INM and MD values of (a) τ_n, the time at which the $C_{vv}(t)$ curve first crosses the x-axis, and (b) τ_m, the time at which the first minimum in the $C_{vv}(t)$ curve occurs. ϵ_{SS} is fixed at 221 K, and temperatures for all the runs are held at 190 ± 5 K.

the behavior of the $C_{vv}(t)$ function for sorbate atoms of sizes 2.67, 4.1, and 6.0 Å, respectively, derived both from the INM spectrum as well as calculated from an MD run. The short-time behavior of the autocorrelation function is well reproduced by the INM result. The agreement between INM and MD curves is better in the anomalous region than in the linear regime. To quantify this comparison between the INM and MD derived $C_{vv}(t)$ curves, we consider two quantities: (i) τ_n, the time at

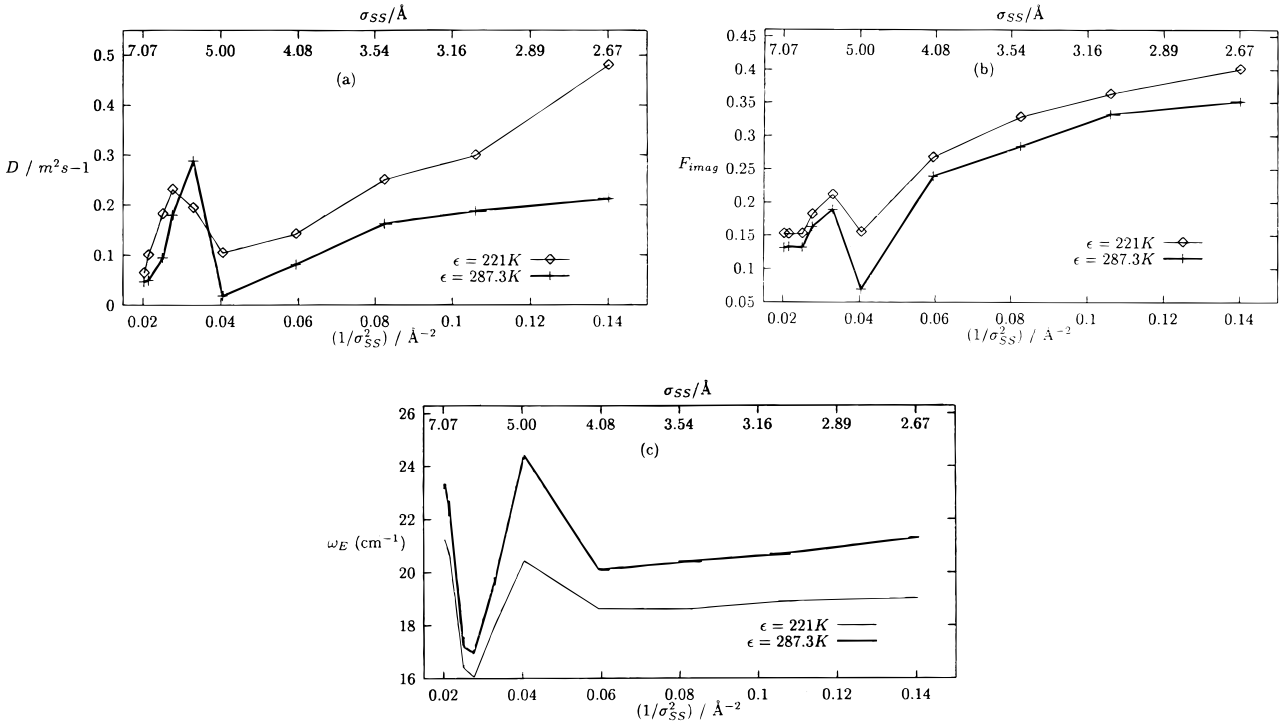

Figure 7. Comparison of (a) self-diffusivity D, (b) fraction of imaginary modes F_{imag}, and (c) Einstein frequency ω_E, as a function of $1/\sigma_{SS}^2$ for ϵ_{SS} values of 221 and 287.3 K. Temperatures for all the runs are held at 190 ± 5 K.

which the vacf curve crosses the abscissa for the first time and (ii) τ_m, the location of first minimum in the vacf curve. We discuss the behavior of these quantities based on the MD results and compare it with the INM predictions.

Figure 6a compares τ_n values derived from the INM expression with the molecular dynamics result. The magnitude of τ_n provides an estimate of the probable time, on average, that a molecule first encounters a repulsive barrier. From the molecular dynamics results, we see that, as sorbate size increases, τ_n initially decreases. At the low concentrations studied in our simulations, this may be attributed to the increasing frequency of collision of a large sorbate with the walls of the cage. This trend in τ_n is reversed in the anomalous regime and a peak is seen at about 6 Å. This signature of the levitation peak in the τ_n values indicates that for favorable sorbate sizes, the system dynamics alters so as to reduce the frequency of repulsive encounters. A comparison of the INM and MD values of τ_n shows that the agreement in the anomalous region is very good which is not surprising in view of the evidence that the dynamics in this regime is strongly dominated by the topography of the potential energy surface. However, for small sorbate sizes in the linear regime, the size-dependent trend in τ_n is not correctly predicted by INM analysis.

The time scale on which a particle reverses its velocity as a result of repulsive encounters is indexed by τ_m, which is shown as a function of sorbate size in Figure 6b. τ_m values are always larger than τ_n, which leads to poorer agreement between the MD result and the INM prediction. For times larger than τ_m, one expects that the INM predictions will not be very reliable.

4.4. Sorbate Polarizability. It is expected that as sorbate polarizability is increased by tuning the parameter ϵ_{SS}, the levitation peak will become more prominent as the effect of the confining potential will be accentuated. However, for large ϵ_{SS}, the sorbate may be essentially trapped at an adsorption site with a self-diffusion coefficient that is virtually zero. This behavior parallels the effect of decreasing temperature on the levitation peak.[12] In our simulations, ϵ_{SS} was varied between

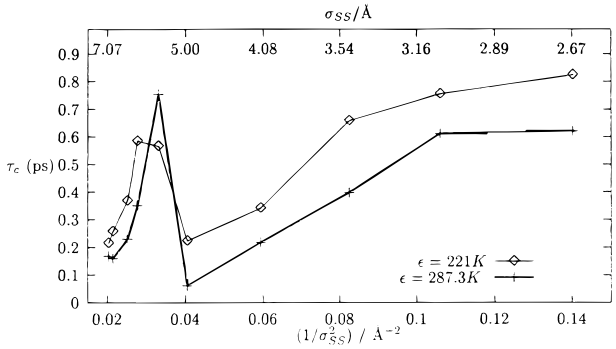

Figure 8. Cross-over times, τ_c, from ballistic to diffusional motion as a function of $1/\sigma_{SS}^2$ for ϵ_{SS} values of 221 and 287.3 K. Temperatures for all the runs are held at 190 ± 5 K.

221 and 442 K. For ϵ_{SS} = 442 K, the values of D were very close to zero. A comparison of the relative values of D, F_{imag}, and ω_E at ϵ_{SS} values of 221 and 287.3 K is shown in Figure 7.

4.5. Ballistic to Diffusional Crossover. It has been observed from previous studies[37] that τ_c, approximate crossover time from ballistic to diffusional regime, is influenced by the nature of the potential energy landscape. The crossover times for ϵ_{SS} = 221 and 287.3 K as a function of $1/\sigma_{SS}^2$ are shown in Figure 8. Note that, as in the earlier studies, the τ_c values also show an anomalous peak. More interestingly, the τ_c values for ϵ_{SS} = 221 K are very close to the τ_n values shown in Figure 6a. Since the cross-over region corresponds to the regime in which the velocity gets randomized as a result of collisional process, this correspondence is quite natural. Note that, for the low sorbate concentrations studied here, these collisonal processes must correspond to sorbate−wall collisons rather than sorbate−sorbate collisions.

5. Conclusions

We have performed an instantaneous normal-mode analysis of the levitation effect for monatomic Lennard-Jones sorbates

adsorbed in Na−Y zeolite. The central conclusion of this study is that the INM spectrum carries several distinct signatures of the levitation effect. The fraction of imaginary modes mirrors the trend in the diffusion coefficient as a function of sorbate size and shows an anomalous levitation peak. Thus, the self-diffusivity constant can be correlated with the extent to which the system samples regions of negative curvature. The Einstein frequency, as a function of sorbate size, shows a minimum at the position of the levitation peak. The qualitative shape of the INM spectrum changes in the anomalous regime, reflecting the availability of 12-ring window sites for adsorption, in addition to the α-cage sites. The velocity autocorrelation functions of the sorbate are well-reproduced from INM data for short time scales of one picosecond, particularly in the anomalous regime. An initial increase in sorbate polarizability accentuates the levitation peak though for large polarizabilities the diffusion constant is negligible for all sorbate sizes. The time of crossover from ballistic to diffusional motion can be approximately predicted from INM spectra since it is found to be similar to the time at which the velocity autocorrelation function first turns negative.

Our instantaneous normal mode analysis of the levitation effect leads one to expect that the INM spectra can be used provide important clues to qualitative changes in diffusional dynamics of sorbates in porous media. We expect INM analysis to be particularly useful when the system dynamics is largely controlled by the topography of the potential energy surface. Since the INM spectrum can be defined in any ensemble, it is therefore worthwhile to couple INM analysis with ensembles and techniques which are more convenient for studying adsorption e.g. the grand-canonical Monte Carlo methods. Qualitative changes in the INM spectra would then indicate significant shifts in the system dynamics which can then be studied more accurately using microcanonical molecular dynamics. Moreover, the INM spectrum could be used to provide insight into the role of various factors such as concentration, nature and strength of confining potential and sorbate properties on diffusional dynamics in porous media.

Acknowledgment. This work was supported by the Indian National Science Academy (Reference BS/YSP-6).

References and Notes

(1) Barrer, R. M. *Zeolites and Clay Minerals as Sorbents and Molecular Sieves*; Academic Press: New York, 1978.

(2) Breck, D. W. *Zeolite Molecular Sieves*; Wiley Interscience: New York, 1974.

(3) Demontis, P.; Suffriti, G. B. *Chem. Rev.* **1997**, *97*, 2845.

(4) Cracknell, R. F.; Gubbins, K. E.; Maddox, M.; Nicholson, D. *Acc. Chem. Res.* **1995**, *28*, 281.

(5) Kärger, J.; Ruthven, D. M. *Diffusion in Zeolites and Other Microporous Solids*; Wiley: New York, 1992.

(6) Hahn, K.; Kärger, J. *J. Phys. Chem.* **1996**, *100*, 316.

(7) Keffer, D.; McCormick, A. V.; Davis, H. T. *Mol. Phys.* **1996**, *87*, 367.

(8) Derouane, E. G.; André, J.-M.; Lucas, A. A. *Chem. Phys. Lett.* **1987**, *137*, 336.

(9) Lambin, Ph.; Lucas, A. A.; Derycke, I.; Vigneron, J. P.; Derouane, E. G. *J. Chem. Phys.* **1989**, *90*, 3814.

(10) Yashonath, S.; Santikary, P. *J. Phys. Chem.* **1994**, *98*, 6368.

(11) Chitra, R.; Yashonath, S. *J. Phys. Chem.* **1998**, *110*, 5960.

(12) Rajappa, C.; Yashonath, S. *J. Chem. Phys.* **1999**, *110*, 1.

(13) Yashonath, S.; Bandyopadhyay, S. *Chem. Phys. Lett.* **1994**, *228*, 284.

(14) Bandyopadhyay, S.; Yashonath, S. *J. Phys. Chem.* **1995**, *99*, 4286.

(15) Wang, Q.; Challa, S. R.; Scholl, D. S.; Johnson, J. K. *Phys. Rev. Lett.* **1999**, *82*, 956.

(16) Stratt, R. M. *Acc. Chem. Res.* **1995**, *28*, 201.

(17) Buchner, M.; Ladanyi, B. M.; Stratt, R. M. *J. Chem. Phys.* **1992**, *97*, 8522.

(18) Stratt, R. M.; Marconelli, M. *J. Phys. Chem.* **1996**, *100*, 12981.

(19) Cho, M.; Fleming, G. R.; Saito, S.; Ohmine, I.; Stratt, R. M. *J. Chem. Phys.* **1994**, *100*, 6672.

(20) Adams, J. E.; Stratt, R. M. *J. Chem. Phys.* **1990**, *93*, 1358; *J. Chem. Phys.* **1990**, *93*, 1632.

(21) Vallauri, R.; Bermejo, F. J. *Phys. Rev. E.* **1995**, *51*, 2654.

(22) Wu, T.-M.; Tsay, S.-F. *J. Chem. Phys.* **1996**, *105*, 9281.

(23) Ribeiro, M. C. C.; Madden, P. A. *J. Chem. Phys.* **1997**, *106*, 8616.

(24) Chakravarty, C.; Ramaswamy, R. *J. Chem. Phys.* **1997**, *106*, 5564.

(25) Cao, J.; Voth, G. A. *J. Chem. Phys.* **1994**, *101*, 6184.

(26) Chakravarty, C. *J. Phys. Chem.* **1997**, *100*, 1878.

(27) Chakravarty, C.; Thiruvengadaravi, K. V. *Proceedings of the Conference on Frontiers in Materials Modelling and Design*; Springer-Verlag: New York, 1997.

(28) Mehra, V.; Basra, R.; Khanna, M.; Chakravarty, C. *J. Phys. Chem. B* **1999**, *14*, 2740.

(29) Bezus, A. G.; Kiselev, A. V.; Lopatkin, A. A.; Pham Quang Du *J. Chem. Soc., Faraday Trans. 2* **1978**, *74*, 367.

(30) Kiselev, A. V.; Pham Quang Du *J. Chem. Soc., Faraday Trans. 2* **1981**, *77*, 1.

(31) Kiselev, A. V.; Lopatkin, A. A.; Shulga, A. A. *Zeolites* **1985**, *5*, 261.

(32) Maitland, G. C.; Rigby, M.; Smith, E. B.; Wakeham, W. A. *Intermolecular Forces: Their Origin and Determination*; Clarendon Press: Oxford, 1981.

(33) Hirschfelder, O. J.; Curtiss, F. C.; Bird, B. R. *Molecular Theory of Gases and Liquids*; John Wiley: Chichester, 1954.

(34) Fitch, A. N.; Jobic, H.; Renouprez, A. J. *J. Phys. Chem.* **1986**, *90*, 1311.

(35) Allen, M. P.; Tildesley, D. J. *Computer Simulation of Liquids*; Clarendon Press: Oxford, 1987.

(36) Frenkel, D.; Smit, B. *Understanding Molecular Simulation: From Algorithms to Applications*; Academic Press: New York, 1996.

(37) Ghosh, M.; Ananthakrishna, G.; Yashonath, S.; Demontis, P.; Suffriti, G. *J. Phys. Chem.* **1994**, *98*, 9354.